CHEMISTRY OF MATERIALS

Article

pubs.acs.org/cm

Understanding the Initial Stages of Reversible Mg Deposition and Stripping in Inorganic Nonaqueous Electrolytes

Pieremanuele Canepa,*[,†] Gopalakrishnan Sai Gautam,[†] Rahul Malik,[†] Saivenkataraman Jayaraman,[†] Ziqin Rong,[†] Kevin R. Zavadil,[‡] Kristin Persson,[§] and Gerbrand Ceder*[,‡]

[†]Department of Materials Science and Engineering, Massachusetts Institute of Technology, Cambridge, Massachusetts 02139, United States

[‡]Sandia National Laboratories, Albuquerque, New Mexico 87185, United States

[§]Environmental Energy Technologies Division, Lawrence Berkeley National Laboratory, Berkley, California 94720, United States

Supporting Information

ABSTRACT: Multivalent (MV) battery architectures based on pairing a Mg metal anode with a high-voltage (~3 V) intercalation cathode offer a realistic design pathway toward significantly surpassing the energy storage performance of traditional Li-ion-based batteries, but there are currently only few electrolyte systems that support reversible Mg deposition. Using both static first-principles calculations and *ab initio* molecular dynamics, we perform a comprehensive adsorption study of several salt and solvent species at the interface of Mg metal with an electrolyte of Mg^{2+} and Cl^- dissolved in liquid tetrahydrofuran (THF). Our findings not only provide a picture of the stable species at the interface but also explain how this system can support reversible Mg deposition, and as such, we provide insights in how to design other electrolytes for Mg plating and stripping. The active depositing species are identified to be $(MgCl)^+$ monomers coordinated by THF, which exhibit preferential adsorption on Mg compared to possible passivating species (such as THF solvent or neutral $MgCl_2$ complexes). Upon deposition, the energy to desolvate these adsorbed complexes and facilitate charge transfer is shown to be small (~61−46.2 kJ mol^{-1} to remove three THF from the strongest adsorbing complex), and the stable orientations of the adsorbed but desolvated $(MgCl)^+$ complexes appear to be favorable for charge transfer. Finally, observations of Mg−Cl dissociation at the Mg surface at very low THF coordinations (0 and 1) suggest that deleterious Cl incorporation in the anode may occur upon plating. In the stripping process, this is beneficial by further facilitating the Mg removal reaction.

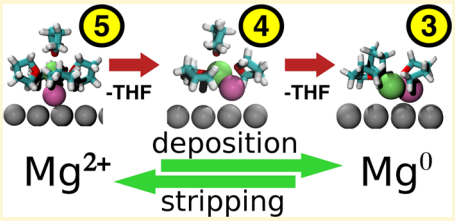

1. INTRODUCTION

Since their commercial introduction nearly 25 years ago, rechargeable Li-ion batteries have performed admirably as the linchpin technology enabling today's mobile electronics industry, currently powering hundreds of millions of laptops, cameras, and phones worldwide.[1] However, after years of continued improvement in performance, we are approaching a fundamental limit of what can be accomplished with the current rocking chair Li-ion battery technology platform.[2] Further improvements in energy density (the quantity of energy that can be stored per charge or discharge either by mass or volume) without increasing the overall cell cost are still required not only to lengthen the per-charge battery life of mobile devices but also to facilitate the widespread adoption of electrified vehicles and grid-scale renewable energy storage. In short, a disruptive innovation in electrochemical energy storage can bring about tremendous technological and societal change: it has the realistic potential to displace significant CO_2 emissions from two of the largest global industrial contributors in transport and electricity generation.

One of the most promising approaches is to build on the traditional robust three-component Li-ion battery architecture (intercalation or metal anode, nonaqueous electrolyte, and intercalation cathode) but with a multivalent chemistry such as Mg^{2+},[3,4] where multiple electrons are transported per ion (i.e., 2 electrons for each Mg^{2+} compared to 1 for Li^+). This feature increases the energy density per intercalated ion in an electrode, but equally important is that along with the switch to a Mg-based chemistry comes the potential to use a Mg metal anode as opposed to an intercalation structure (~700 Ah/L for Li in graphite compared to 3830 Ah/L for metallic Mg). For Li, the use of metallic anodes is especially challenging for safety reasons.[5]

The path to fully functioning and cost-competitive Mg-ion batteries begins with addressing a few but complex scientific questions, of which perhaps the most pressing is to develop a robust understanding of the atomistic mechanism of reversible plating (or deposition) and stripping (or dissolution) of Mg at the anode/electrolyte interface during battery operation. To date, reversible Mg plating with low overpotential and reasonable anodic stability has been achieved in practice with only a specific class of electrolytes, namely, organic or inorganic

Received: January 30, 2015
Revised: April 8, 2015
Published: April 8, 2015

DOI: 10.1021/acs.chemmater.5b00389
Chem. Mater. 2015, 27, 3317−3325

magnesium aluminum chloride salts (magnesium−chloro complexes) dissolved in ethereal solvents.[6−11] Aurbach and collaborators developed the first operational Mg ion full cells using electrolytes based on Grignard reagents (e.g., butylmagnesium chloride)[6] and improved upon their performance by switching to an in situ prepared magnesium organohaloaluminate, which can achieve high Coulombic efficiency during stripping and deposition and anodic stability up to 3.0 V.[7,8,11] Recently, Muldoon and co-workers further improved upon air sensitivity and anodic stability by designing a non-nucleophilic electrolyte containing a Hauser base, such as hexamethyldisilazide magnesium chloride (HMDSMgCl) and $AlCl_3$.[12] Another functioning electrolyte, though displaying limiting anodic stability, can be achieved using a combination of $Mg(BH)_4$ and $LiBH_4$ in diglyme, as demonstrated by Shao et al.[13] Despite this substantial progress, some aspects of the electrolytes are in need of improvement, particularly the anodic stability, safety, and compatibility with other cell components.[14] In contrast, most other nonaqueous electrolytes, including the Mg analogues to the common Li-ion battery electrolytes, lead to immediate electrolyte decomposition on the Mg anode, which passivates the metal surface, preventing further electrochemical reactions.[3]

Much effort has been devoted toward characterizing the precise sequence of atomic-scale processes that make up the overall Mg deposition/dissolution process in ethereal solvents. First, extensive experimental and computational approaches have been used to characterize the equilibrium solvation structure of Mg^{2+} in the bulk electrolyte, which defines the thermodynamic start (end) point of deposition (dissolution), and several possible coordinating complexes involving combinations of Mg^{2+}, Cl^-, and THF have been identified.[7,8,10,11,15−18] These findings have subsequently been used to inform phenomenological models that describe the general sequence of ion desolvation, adsorption on the anode surface, charge transfer, and metal incorporation that make up the overall deposition process (the sequence in reverse describes the dissolution process; in ref 11 and references therein). Only if all of these individual processes are kinetically unobstructed can an Mg anode operate reversibly and efficiently, e.g., with low overpotential and high Coloumbic efficiency.

However, the complete understanding on the atomic scale of the processes of electrochemical plating and stripping at the Mg anode/electrolyte interface, which would enable rational design of the next-generation Mg-based electrolytes, is still lacking. In recent work, Doe et al.[8] showed that purely inorganic-based electrolytes solutions (i.e., without organometallic moieties), also referred as the MACC electrolyte, can exhibit reversible Mg electrodeposition with anodic stability up to 3.1 V vs Mg. Hence, the MACC electrolyte system can serve as an excellent prototype system to understand Mg deposition and stripping in the presence of Mg−Cl complexes. Here, we present an in-depth first-principles study aimed at characterizing the relevant chemical structures and complexes that form at the interface of a Mg metal anode in contact with an electrolyte solution composed of Mg^{2+} and Cl^- dissolved in an ether-based solvent (tetrahydrofuran or THF). By performing static first-principles adsorption calculations combined with *ab initio* molecular dynamics (AIMD) simulations, we are able to separately probe the interaction of the THF solvent in contact with the anode surface as well as the full electrolyte/anode interaction by incorporating both Mg^{2+} and Cl^-. Combined, these calculations reveal important features about magnesium−chloro complexes and their ability to function in practice: first, cyclic ether-based solvents are confirmed to be chemically inert against the Mg anode, whereas polymer-like ethers display comparatively more passivating behavior on the Mg anode; second, our calculations reveal the existence of several $(MgCl)^+$ coordination complexes similar in energy but solvated by different numbers of THF molecules that define a kinetically facile Mg^{2+} desolvation process during deposition.

The computational and theoretical strategy used to gain insights into the species at the Mg anode electrode and Mg desolvation/dissolution is nonspecific and can be readily applied to a variety of important problems such as electroforming of metals, corrosion of metals and alloys, medicinal chemistry, and catalysis. We emphasize that to obtain physically meaningful results, we consider explicitly the interaction of nonaqueous liquids with a solid phase, which is commonly approximated by a vapor/solid interface in other studies.

2. METHODOLOGY

Absorption calculations and *ab initio* molecular dynamics (AIMD) simulations were performed within the DFT approximation, using the vdW-DF functional[19,20] as implemented in VASP.[21,22] The total energy was sampled on a well-converged 3 × 3 × 1 *k*-point grid together with projector-augmented wave theory[23] and a 520 eV plane-wave cutoff, and forces on atoms were converged within 1×10^{-2} eV $Å^{-1}$. For the different adsorption geometries of Figures 1 and 5a, the adsorption energy (ΔE) is defined as

$$\Delta E = E_{\mathrm{surf+ads}}(\mathrm{s}) - E_{\mathrm{surf}}(\mathrm{s}) - E_{\mathrm{ads}}(\mathrm{l}) \quad (1)$$

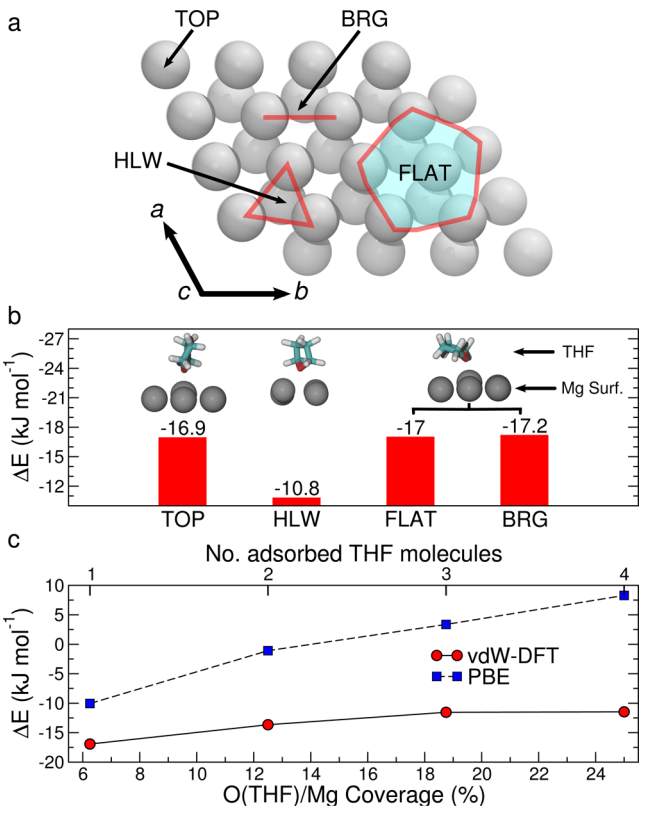

Figure 1. (a) Stable adsorption sites (TOP, HLW, FLAT, and BRG) for THF on Mg(0001) and corresponding (b) adsorption energies ΔE (in kJ mol^{-1} referenced to the THF liquid state) with snapshots of their fully relaxed THF configurations (inset). (c) Variation of the adsorption energy with THF surface coverage O(THF)/Mg.

DOI: 10.1021/acs.chemmater.5b00389
Chem. Mater. 2015, 27, 3317−3325

where the $E_{surf+ads}(s)$ is the total energy of the species formed by the Mg surface and the adsorbing molecule (solvent or salt) in the solid state, $E_{surf}(s)$ the total energy of the surface in the solid state, and $E_{ads}(l)$ the total energy of the n adsorbing species. $E_{ads}(l)$ is conventionally approximated by the total energy of its gas reference, but to address the specific problem of the electrode in contact with a liquid electrolyte, it is more practical to refer to the liquid state. To compute the liquid reference $E_{ads}(l)$, we proceed by isolating low-energy snapshots from AIMD runs of both salt ($MgCl^+$ or $MgCl_2$ in THF solvent) and solvent (THF) and optimize their geometries. The average total energy provides a good estimate of the liquid reference and incorporates both stabilizing first solvation shell effects and vdW effects from the solvent.

As the coordination of $(MgCl)^+$ by THF in bulk is still debated, two different liquid $(MgCl)^+$ bulk references were computed: (i) four-coordinate Mg, $(MgCl)^+$−3THF, as determined by Wan et al.,[16] and (ii) six-coordinate Mg, $(MgCl)^+$−5THF, as proposed by previous experimental work.[8,10,11,15,17]

For the AIMD calculations, the cutoff was reduced to 400 eV and the total energy was sampled only at the Γ-point. Using a sampling of 1 fs, a production period of 15 ps was preceded by an equilibration period of 20 ps within the canonical ensemble (NVT) at 300 K, using the Nosé−Hoover thermostat.[24,25] The slabs for the adsorption calculations were cleaved from the fully relaxed geometry of the Mg bulk (with a = 3.202 Å and c = 5.139 Å) and MgO (with a = 4.201 Å). Mg(0001) and MgO(100) surfaces were modeled using a five-layer periodic slab. Specifically, for the adsorption of THF and poly-THF, a 4 × 4 ($a = b$ = 12.808 Å) slab with 80 Mg atoms was employed, whereas a 2 × 2 ($a = b$ = 8.931 Å) slab with 90 atoms was used for MgO. For the adsorption of $(MgCl)^+$ and $MgCl_2$ complexes, a larger surface with a size of 5 × 5 ($a = b$ = 16.010 Å) and 125 Mg atoms is needed. A well-converged vacuum of 35 Å was inserted between surface images, and the adsorbing species were always adsorbed on both surfaces to minimize artificial electric dipoles through the nonperiodic direction of the slab. The atomic positions of the two most exposed layers of the slabs and the adsorbates were optimized. All geometries employed in the AIMD simulations were created by inserting a number of THF molecules at the experimental density (0.889 g/cm^3) in the vacuum space between slabs to simulate liquid, resulting in unit cells with ∼550 atoms. To accelerate computationally costly AIMD simulations, we performed an intermediate 1 ns pre-equilibration NVT classical molecular dynamics simulation using the CHARMM potential, as implemented in DL_POLY,[26,27] while keeping the coordinates of the surface and adsorbate atoms fixed, as obtained from preliminary adsorption calculations. The concentration of the $MgCl^+$ salt in the AIMD is 0.30 M and falls in the range of the experimental concentrations of 0.25−0.40 M explored by Aurbach and collaborators.[28] Diffusivities were extracted from the mean-squared displacements of the molecules at the surface from the AIMD simulations.

3. RESULTS

3.1. THF on Mg. Adsorption energies computed from first-principles calculations are used to quantify the chemical interaction of a solvent tetrahydrofuran (THF) molecule with the Mg metal anode. From the standpoint of electrostatic interaction, the THF molecule is expected to preferentially align with the ethereal oxygen oriented toward the exposed Mg sites at the surface. Previous experimental[29] and theoretical[30] work has demonstrated that Mg deposition and growth occur preferentially on the Mg(0001) facet at low current densities (∼0.5−1.0 mA cm^{-2}); hence, the analysis is restricted to the Mg(0001) surface. Figure 1a,b shows four plausible adsorption sites at the Mg(0001) surface for a THF molecule, labeled TOP, BRG, HLW, and FLAT, and their adsorption energies (ΔE). In this article, we refer strictly to the hcp hollow site HLW, as indicated by the triangle in Figure 1a, as opposed to the less stable fcc hollow site, which shows consistently weaker adsorption energies.

The calculated adsorption energies of Figure 1b (referenced to liquid THF) fall into a narrow range between −10 and −17 kJ mol^{-1} with negligible variation between distinct surface sites and are consistent with the inert nature of ethereal molecules in the presence of a highly electropositive metal.[3,11,31] Negative ΔE's indicate that spontaneous adsorption is preferred. Referencing to the THF gas state would make the adsorption energies more negative (see Supporting Information Figure S1) by adding the gas to liquid bonding energy (∼−46 kJ mol^{-1}). The lower ΔE (∼−17.2 kJ mol^{-1}) of the FLAT configuration originates from the THF molecule's orientation at the surface, favoring not only the O−Mg(surface) interaction (of the top configuration) but also additional weaker C−Mg(surface) and H−Mg(surface) bonds. THF molecules initially adsorbed in the BRIDGE sites are found to relax to the FLAT configuration (Figure 1b).

A more realistic picture of THF adsorption, consistent with experimental conditions, is achieved by considering the effect of THF coverage. Figure 1c shows the variation of the adsorption energies for increasing number of adsorbed THF. The interaction of THF with the surface noticeably decreases with increasing THF coverage, and the adsorption energies shift to further positive values consistent with the occurrence of THF−THF lateral electrostatic repulsions. As a comparison, we also report ΔE's that do not include van der Waals interactions (marked PBE in Figure 1c), which provide a helpful upper-bound limit for the adsorption energies. The entropic contributions originating from the THF adsorption from the liquid will further increase the adsorption free energies to more positive values, displacing the THF molecule from the Mg anode and ensuring that ether molecules do not passivate the surface.

To test the findings provided by the adsorption calculations and further resolve the dynamic environment of the anode/solvent interface, AIMD simulations within the canonical ensemble were performed at room temperature (300 K) and at the experimental density of THF (0.889 g/cm^3).[28] Figure 2a (black line) shows the pair distribution function, PDF or $g(r)$, of the exposed Mg surface sites versus the THF oxygen atoms, Mg_{surf}−O.

The two dominating peaks observed at ∼2.0 and 2.5 Å show the coexistence of two THF configurations at the Mg(0001) surface, FLAT (peak at ∼2.0 Å) and TOP (peak at ∼2.5 Å), which also have the most negative adsorption energies, as seen in Figure 1b. By integrating the PDF profiles of Figure 2a (red line), we conclude that a maximum of four THF molecules (2 in FLAT and 2 in TOP conformation) per 16 Mg exposed surface sites can be simultaneously adsorbed (dashed red line in Figure 2a), consistent with the adsorption results of Figure 1c. The diffusivity of THF molecules at the surface extracted from their mean-squared displacement observed in the AIMD simulation is (6.1 ± 1.5) × 10^{-6} cm^2 s^{-1}. Physically, the mean-squared displacement of a molecule at the metal surface is related to the strength of adsorption: if the interaction is very strong (attractive), then molecules near the surface remains predominantly in the adsorbed state rather than in the liquid, resulting in lower surface diffusivity.

3.2. Poly-THF on Mg. It is well-understood that either electrophilic attack by protons on the ethereal carbon (self-polymerization) or catalytic interaction with an electropositive metal (such as Al in $AlCl_3$ or Mg) can initiate the THF ring

DOI: 10.1021/acs.chemmater.5b00389
Chem. Mater. 2015, 27, 3317−3325

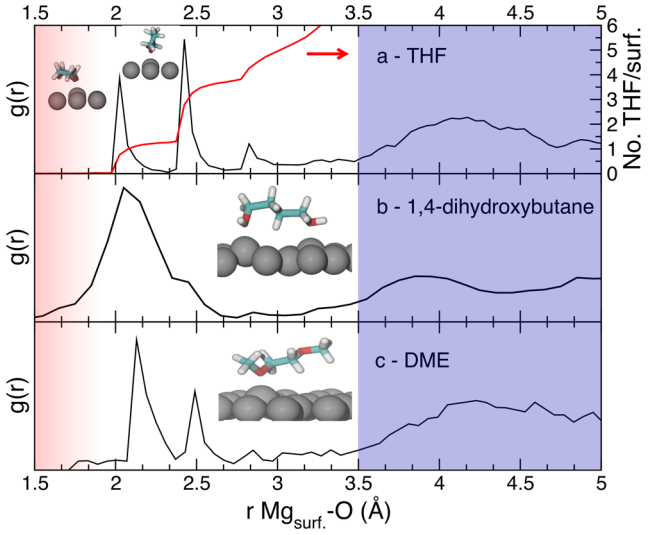

Figure 2. PDF, $g(r)$, of ethereal oxygen of THF and exposed Mg(0001) surface atoms (black lines) and surface coverage (dashed red line) for (a) THF, (b) 1,4-dihydroxybutane, and (c) DME (1,2-dimethoxyethane) from AIMD simulations. Insets are representative snapshots of THF and poly-THF fragments at the Mg surface. Red and blue shades highlight the lower bound of PDFs and the 2nd solvation shell, respectively.

opening, followed by polymerization, forming poly-THF.[10,32,33] We therefore also investigate the possible adsorption of THF products of polymerization such as polytetrahydrofuran (poly-THF) at the anode/electrolyte interface shown in the inset of Figure 2b. Here, two approximations are used to describe poly-THF: (i) by cleaving THF at the ethereal bonds and saturating with hydrogen atoms, forming the 1,4-dihydroxybutane (Figure 2b), and (ii) by 1,2-dimethoxyethane, also known as glyme (DME, Figure 2c). While the acidic nature of the terminal hydrogens in 1,4-dihydroxybutane may enhance the adsorption energy with the Mg surface compared to linear ethers (e.g., glyme, tetraglyme, *n*glyme), it nonetheless provides an upper bound to the adsorption energies of a variety of THF polymerization products that might be present in the cell. The adsorption energies of 1,4-dihydroxybutane (referencing to a dilute solution of 0.4 M 1,4-dihydroxybutane-THF in liquid THF) for different configurations were always found to be more negative (-32.0 ± 5 kJ mol^{-1}) than those of cyclic THF (-17.2 kJ mol^{-1}). Examination of the Mg$_{surf}$–O PDF reveals that the oxygen atoms of 1,4-dihydroxybutane are always nearer to the Mg surface (broad peak from 1.7 to 2.7 Å) in comparison to cyclic THF molecules (Figure 2a,b), likely due to more geometric degrees of freedom accessible by 1,4-dihydroxybutane that can allow for improved binding for a linear molecule on the anode surface. Measurements of the diffusion coefficients (from AIMD simulations) further indicate a smaller mobility of 1,4-dihydroxybutane at the surface, $\sim(9.5 \pm 1.6) \times 10^{-7}$ cm^2 s^{-1}, as compared to weakly physisorbed and more mobile THF molecules, $\sim(6.1 \pm 1.5) \times 10^{-6}$ cm^2 s^{-1}. However, at the Mg(0001) surface, DME is found to bind less strongly (-10.5 ± 1 kJ mol^{-1}) than 1,4-dihydroxybutane (-32.0 ± 5 kJ mol^{-1}) and comparable to THF (-17.2 kJ mol^{-1}), confirming the inert nature of this molecule. Although the similarity of the Mg$_{surf}$–O PDFs of DME and THF (Figure 2a,c) attests to a comparable binding nature for these molecules, the minimum distance between the ethereal oxygen of DME and Mg atoms at the surface falls at slightly larger distances (see peak at 2.1 Å) than in THF (see peak at 2.0 Å in Figure 2a), which can be explained by the larger steric hindrance of DME.

Recently, Barile et al.[10] observed that the addition of poly-THF in MACC electrolyte increases the deposition over-potentials to 500 mV, indicating that poly-THF may passivate the Mg surface more. We conclude that hydroxyl-terminated polymer molecules (e.g., 1,4-dihydroxybutane) are more prone to passivate the Mg anode surface (than linear ethers and THF), thereby negatively affecting the battery's performance during stripping and deposition. Furthermore, the chelating nature of linear ether with long chains (e.g., glyme, diglyme, tetraglyme, and poly-THF) is expected to inhibit Mg^{2+} ion delivery at the surface.[34,35]

3.3. THF on MgO. The irreversible reaction of Mg with ubiquitous water forms resistant passivation layers that suppress all Mg electrochemical activity and is one of the limiting factors in the development of Mg-ion batteries. Investigations of Mg corrosion have clarified the bilayer structure of the passivating film, with the inner part composed of MgO and an external layer of $Mg(OH)_2$.[31,36,37] In order to clarify the effect of surface passivation on solvent adsorption, we calculated the adsorption energies for THF on the MgO(100) termination,[38] which is found to grow epitaxially on the Mg(0001) facet. Analogous to previous sections, we use static DFT adsorption calculations to address the interaction of THF with MgO(100) and verify these findings with auxiliary *ab initio* MD simulations. We anticipate that the ethereal oxygen of THF will interact preferentially with Mg atoms at the surface (as also seen by THF on Mg metal), whereas THF's H atoms will maximize H-bonding with surface oxygens.

Figure 3a,b shows four plausible adsorption sites at the MgO(100) surface for a THF molecule, labeled TOP, FLAT, BRG, and BRG-H, and their respective adsorption energies (ΔE). BRG-H represents a THF adsorption arrangement that maximize H-bonding between THF hydrogen atoms and MgO oxygen species at the interface (Figure 3a). TOP, FLAT, and BRG configurations are the same as those described for adsorption on Mg.

Surprisingly, the adsorption energies reported in Figure 3b (referenced to liquid THF) are found to be remarkably close to ΔE's computed for THF on Mg(0001), varying between -17 and -18 kJ mol^{-1}. By close examination of each THF adsorption configuration and relative ΔE's, we observe that the BRG configuration relaxes to TOP and, similarly, the FLAT configuration relaxes to BRG-H, which maximizes the interactions with the surface oxygen atoms through hydrogen bonds (snapshots in Figure 3b). On the basis of these results, we cannot observe a substantial difference between the adsorption properties of THF on MgO(100) and Mg(0001) surfaces and suggest that further theoretical and experimental investigations are needed.

AIMD simulations are performed to investigate the dynamic properties of THF molecules at the MgO interface with similar settings as those described in previous sections. Figure 4a,b (black line) shows the pair distribution functions, PDF or $g(r)$, of the exposed Mg and O surface sites versus the THF oxygen atoms, Mg$_{surf}$–O$_{THF}$ and O$_{surf}$–O$_{THF}$, respectively.

Similar to Figure 2, the Mg$_{surf}$–O$_{THF}$ PDF of Figure 4a shows two major peaks at ~2.0 and 2.5 Å, emphasizing the coexistence of two THF adsorption configurations at the MgO(100) surface: BRG-H (peak at ~2.0 Å) and TOP (peak at ~2.5 Å). The remarkable similarity of the Mg$_{surf}$–O PDFs on

DOI: 10.1021/acs.chemmater.5b00389
Chem. Mater. 2015, 27, 3317–3325

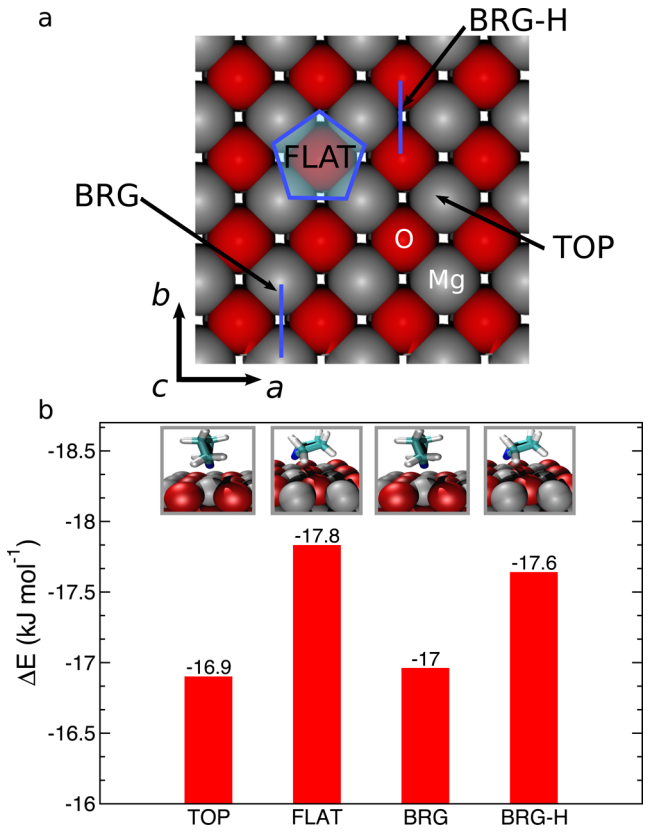

Figure 3. (a) Stable adsorption sites (TOP, FLAT, BRG, and BRG-H) for THF on MgO(100) and corresponding (b) adsorption energies ΔE (in kJ mol^{-1} referenced to the THF liquid state) with snapshots of their fully relaxed THF configurations (inset). THF ethereal oxygen in blue for clarity.

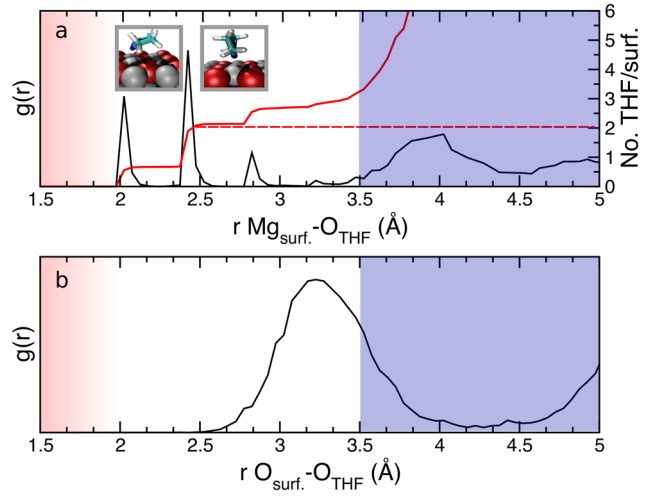

Figure 4. (a) PDF, $g(r)$, of ethereal oxygen of THF and exposed Mg surface atoms and (b) O exposed surface atoms on MgO(100) (black lines) (coverage, dashed red line). Insets are representative snapshots of THF fragments at the MgO surface. Red and blue shades highlight the lower bound of PDFs and the 2nd solvation shell, respectively.

Mg(0001) and MgO(100) (compare Figures 2a and 4a) suggests that PDF analysis is not sufficient to distinguish whether THF molecules are adsorbed on active or passivated Mg anodes. The PDF O_{surf}–O_{THF} shown in Figure 4b is more informative and can discriminate between adsorption on active or passivated surfaces, with a single peak between 2.7 and 4.0 Å characteristic of absorption on MgO. Mg_{surf}–O_{THF} PDF also provides information about the THF coverage on MgO (red line in Figure 4a), concluding that a maximum of two THF molecules (1 in FLAT and 1 in BRG-H conformation) can be simultaneously adsorbed per 12 Mg exposed surface sites (dashed red line in Figure 4a).

3.4. Magnesium–Chloro Salt and THF Solvent. By first establishing that ethereal solvent molecules do not significantly interact with the Mg anode surface, we turn our attention to characterizing the anode/electrolyte interface by including the magnesium chloride salt species (solvated by THF). The atomic-scale interactions between salt and solvent that define the relevant reacting complexes and species in the bulk electrolyte can be quite complex, as demonstrated in seminal work by Aurbach and collaborators, who characterized intricate equilibria between magnesium–chloro clusters and $AlCl^{4-}$ in the form of simpler monomers $[Mg(\mu\text{-}Cl)\cdot 5THF]^+[(AlCl_4)]^-$, dimers $[Mg_2(\mu\text{-}Cl)_3\cdot 6THF]^+[(AlCl_4)]^-$, and larger polymeric species.[7,8,10,15,17] A recent theoretical work by Wan et al.[16] clarified the first solvation shell of the monomer and dimer magnesium organo–chloro species in the bulk electrolyte. Their AIMD calculations suggest that the $(MgCl)^+$ monomer is always coordinated by three THFs. However, it is still debated whether the $(MgCl)^+$ monomer is actively present in the bulk electrolyte or only formed in proximity of the electrode as a product of dimer decomposition.[17] The structure of the organo–chloroaluminate salts $(C_2H_5MgCl–[(C_2H_5)_2AlCl]_2$ in THF, dichloro complex) in proximity of the Mg anode was investigated experimentally using XANES spectroscopy by Benzmayza et al.,[17] revealing that only the cation monomer $[Mg(\mu\text{-}Cl)\cdot 5THF]^+$ can approach the surface (as opposed to the more complex and bulkier dimer and trimer), thus representing the active species during Mg deposition. Previous work[7,10,15,17] on the organo and inorgano chloroaluminate electrolytes has elucidated the complex thermodynamic equilibria among monomer, dimer, and larger multimeric species, which might ultimately affect the concentrations of $(MgCl)^+$ near the anode electrode. Even though more complex Mg carriers (e.g., dimer and larger multimeric units) could also be present at the surface, we set to investigate only the monomer $(MgCl)^+$ as the simplest possible vehicle to transport Mg^{2+} ions from the electrolyte in proximity of the anode.[10] In this work, we use these findings to inform the construction and preparation of our first-principles simulations, focusing on the interaction of $(MgCl)^+$ monomers coordinated by THF near the anode surface.

Using a similar approach to the one used to study the anode/solvent interface, we first probe the adsorption energies of possible magnesium–chloro complexes and then perform AIMD simulations to explore more precisely the dynamic nature of the anode/electrolyte salt interface. Envisioning the overall Mg deposition process, for example, beginning with a THF-solvated $(MgCl)^+$ complex in the bulk electrolyte and ending as metallic Mg incorporated in the anode, the deposited Mg must, in some sequence, shed its sheath of THF molecules. In Figure 5, the interfacial structure and corresponding adsorption energies of several charged magnesium–chloro $(MgCl)^+$ complexes (solvated by 5 through 0 THF molecules and in different orientations) adsorbed on a Mg(0001) surface are shown. Throughout the article, we adopt an abbreviated nomenclature to discuss magnesium–chloro $(MgCl)^+$ complexes adsorbed at the Mg surface, namely, the first number

DOI: 10.1021/acs.chemmater.5b00389
Chem. Mater. 2015, 27, 3317–3325

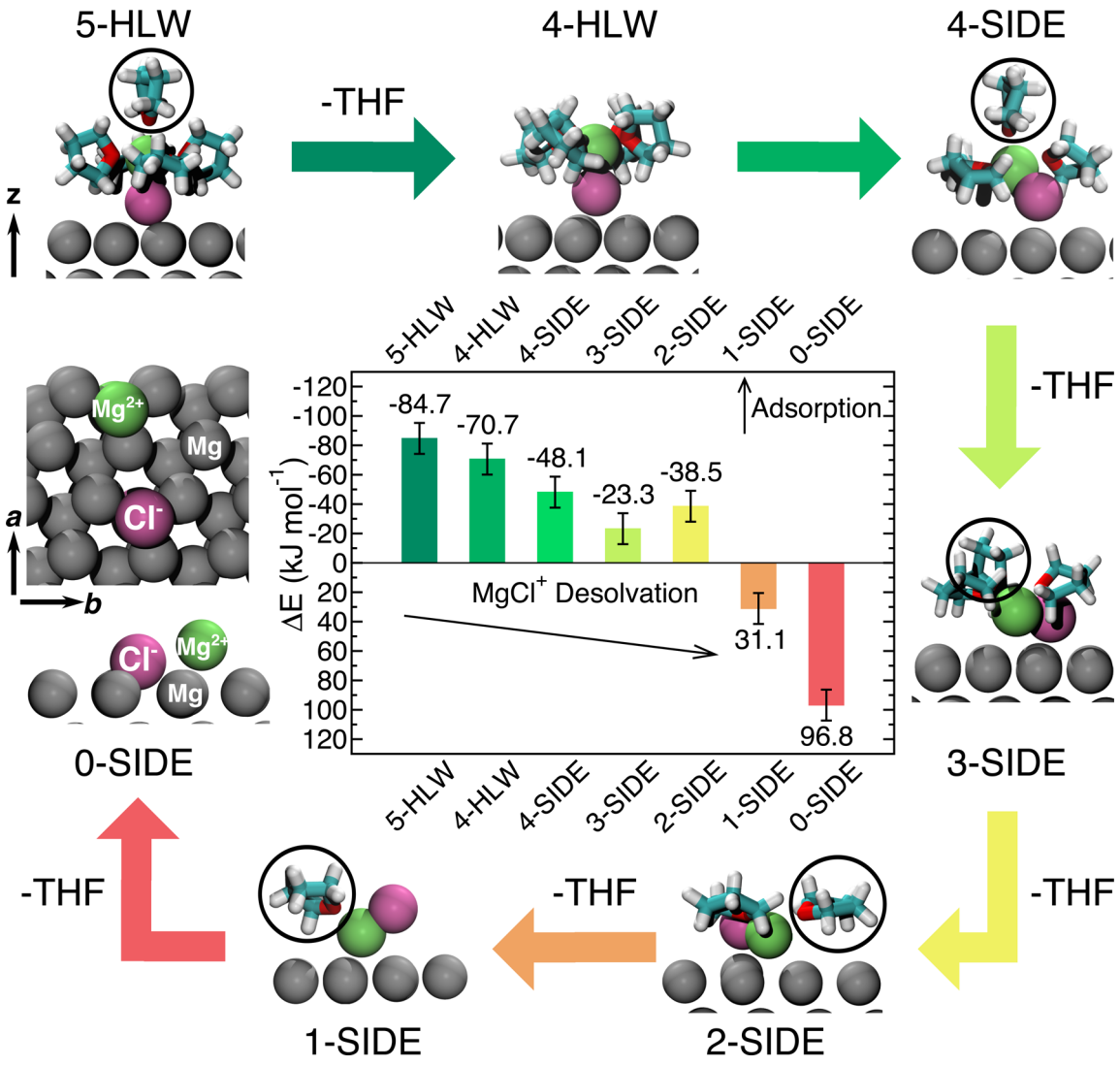

Figure 5. Stable configurations of $(MgCl)^+$ solvated by varying the number of THF (from 5 to 0) adsorbed at the Mg(0001) surface and corresponding adsorption energies (ΔE in kJ mol^{-1}). Upper and lower bounds indicated by the bars on ΔE's are from using 3-THF and 5-THF bulk liquid reference states, respectively. Black circles and color-coded arrows indicate THF removal.

indicates the number of THF ligands followed by the orientation (or site) adopted by the adsorbing $(MgCl)^+$ salt. For example, 4-SIDE means that $(MgCl)^+$ is coordinated by 4-THF molecules and lays horizontally on the Mg surface, as shown in the snapshots in Figure 5. Two different liquid references were used to compute the ΔE's of adsorbed magnesium−chloro salts at the Mg surface: (i) bulk $(MgCl)^+$−3THF reference[16] and (ii) with a bulk $(MgCl)^+$−5THF,[7,17] as indicated, respectively, by the upper and lower bounds of the bars in Figure 5. The difference in absorption energies from these two reference states is small and can be attributed to the slightly more stable $(MgCl)^+$−3THF reference in the reference calculation.

Upon first inspection, the magnitude of the energies for salt adsorption (Figure 5) compared to THF adsorptions (values shown in Figure 1b and text above) confirms that the THF solvent weakly interacts with the Mg metal surface, whereas magnesium−chloro salt complexes readily adsorb, in good agreement with experimental observations by Benzmayza et al.[17] and the reversible plating is observed in this system.[3,7,8,10,11] In all cases, Cl aligns toward the Mg surface, with adsorption on the HLW site preferred over the TOP site, as shown in Figure 1 (also see Figure S2 in Supporting Information), because in comparison to TOP, HLW- and SIDE-oriented adsorption (Figure 5) maximizes the interaction of the Cl ion with the Mg surface sites as well as that of some dangling C and H atoms from the THF molecules with the Mg surface. Of all the charged magnesium−chloro complexes, $(MgCl)^+$ coordinated by 5 THF in the hollow site exhibits the strongest adsorption energy (-84.7 ± 10.5 kJ mol^{-1}) and, in general, the strength of the adsorption reduces with sequential THF removal, as seen in the trend of adsorption energies of Figure 5. Also, as THF is successively removed from the salt complex, the most stable orientation relative to the surface shifts from HLW to SIDE. Both trends can be understood by considering the role of the Mg surface in stabilizing known preferred Mg^{2+} coordination geometries.[17] For 5-HLW, Mg^{2+} can remain stably in octahedral coordination, as seen in Figure 5, but as more THF molecules are removed, Mg^{2+} is increasingly exposed to unstable coordinations. For a comparative example, 4-HLW has a more positive adsorption energy. Adopting the SIDE orientation allows Mg^{2+} to be

DOI: 10.1021/acs.chemmater.5b00389
Chem. Mater. 2015, 27, 3317−3325

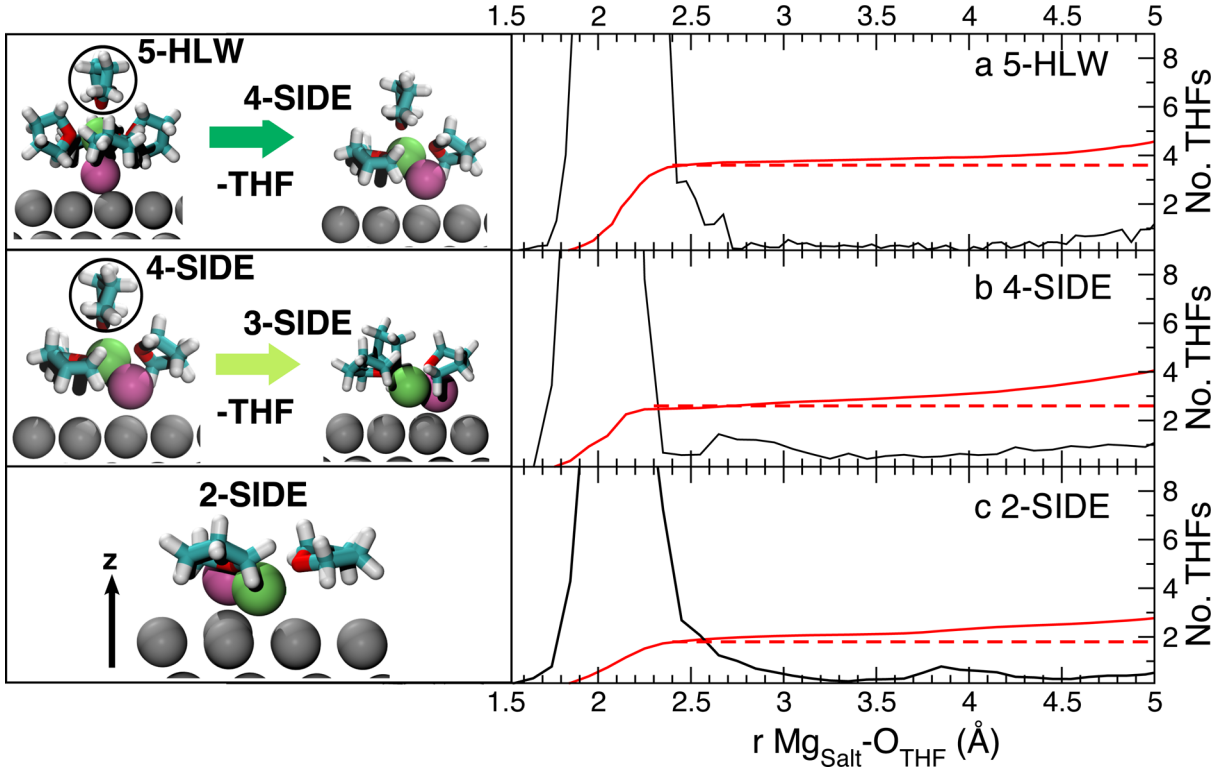

Figure 6. PDFs, $g(r)$, and coordination number of Mg atoms in the $(MgCl)^+$ salt and THF oxygen atoms for models (a) 5-HLW, (b) 4-SIDE, and (c) 2-SIDE (Figure 5). Insets show the structural evolution of the salts at the surface. Red dashed lines are a guide for the eye. Black circles indicate THF removal. Mg−Cl PDFs are in Figure S4 of the Supporting Information.

additionally coordinated by the Mg surface, which can stabilize the salt complex when there are too few THFs to ideally solvate Mg^{2+}, as seen in Figure 5, where the SIDE configuration becomes the most stable for 3 THFs or fewer. As even more THF molecules are removed, the adsorption of the salt complexes is continually weakened, but a notable exception is from 3-SIDE to 2-SIDE (Figure 5), where there is an increase in adsorption strength, likely due to less steric hindrance between THF molecules, which can be relieved by removing the most weakly bound THF. The adsorption of $(MgCl)^+$−1THF, 1-SIDE and bare $(MgCl)^+$, 0-SIDE on the Mg(0001) surface was found to be very unfavorable (+31.1 and +96.8 kJ mol^{-1}, respectively), indicating that these species are likely too unstable to play a significant role in the reversible Mg deposition process.

As mentioned earlier, the $(MgCl)^+$ monomer surrounded by a solvent coordination shell of 4 or 5 THF molecules adsorbs strongly to the Mg surface (Figure 5), but these complexes also preserve the integrity of the weak Mg−Cl bond. In addition to electron transfer, completion of the Mg deposition process also requires the eventual dissociation of Mg from Cl^- at the Mg surface, which necessitates breaking the solvation shell. The differences in adsorption energies shown in Figure 5 can also be considered as the energy to (de)solvate the $(MgCl)^+$ complex by sequential (removal) addition of THF molecules, and initial desolvation appears to be facile with only a cumulative ∼46.2−61.0 kJ mol^{-1} required to remove 3 THFs from the stably adsorbed $(MgCl)^+$−5THF complex. To investigate this observation further under more realistic conditions comparable to experiment, we perform room-temperature AIMD simulations with different $(MgCl)^+$ complexes adsorbed on the Mg surface in a liquid THF reservoir. Figure 6 shows the pair distribution function between the Mg atom of the $(MgCl)^+$ salt and the oxygen atoms of the THF ligands (black lines) and the respective coordination numbers (red lines) for three different salt adsorption configurations, 5-HLW, 4-SIDE, and 2-SIDE. In Figure 6, the average Mg_{Salt}−O_{THF} distance is centered around 1.8−2.2 Å, falling in the typical Mg−O bond length range (2.1−2.2 Å). The coordination number measured at the center of the $g(r)$ peaks (see red dashed lines in Figure 6 as a guide for the eye) is 4, 3, and 2 for 5-HLW, 4-SIDE, and 2-SIDE, respectively.

Surprisingly, in some cases, the number of THFs in the first coordination shell of the $(MgCl)^+$ salt spontaneously decreases by one THF unit after a few picoseconds of equilibration time in the AIMD simulation. For example, when beginning the AIMD simulation with either 5-HLW or 4-HLW absorbed on the Mg surface, we observe 4-HLW and 3-SIDE as the final result, respectively, as seen in the dashed red lines in Figure 6a,b. This is likely due to additional THF−THF interactions between the ligands of the adsorbed complex and bulk liquid in the AIMD simulation (unaccounted for in the static adsorption calculations, which are performed in vacuum) and the effect of entropy, which stabilizes THF in the liquid compared to the adsorbed state. This evidence further supports Mg ion desolvation as a facile process. As seen in Figure 6, the trend of spontaneously shedding THF stops in the 2-SIDE configuration, as the significant increase in desolvation energy required to further remove THF (Figure 5) cannot be offset by finite temperature and additional solvent interactions.

The large positive energy increases when removing additional THF, i.e., from 2-SIDE to 1-SIDE to 0-SIDE, suggests that the electron transfer likely occurs before, when there are still some surrounding THF molecules (likely 2), which further

DOI: 10.1021/acs.chemmater.5b00389
Chem. Mater. 2015, 27, 3317−3325

underscores the necessity of considering the stabilizing coordination effect of the solvent ion with an explicit 1st coordination shell of THF. From close inspection of the relaxed geometries of low and zero-coordinated THF complexes (such as adsorbed 1-SIDE and 0-SIDE, Figure 5), we observe incipient dissociation of the Mg−Cl bond. This also occurs for some of the $MgCl_2$ configurations (see Figure S5 in the Supporting Information), which further suggests that magnesium−chloro complexes with few THF molecules are the relevant species involved in charge transfer. Fortunately, the SIDE orientation is most energetically favorable at lower THF coordinations (Figure 5), which allows for the depositing Mg^{2+} to become better exposed to the anode surface, which should better facilitate ensuing charge transfer.

Finally, we also consider the adsorption on the Mg surface of the charge-neutral $MgCl_2$ species that may precipitate at the anode interface, for example, as undissolved/unreacted $MgCl_2$ during the preparation and possibly conditioning[10] of the magnesium−chloro electrolyte. Previous AIMD simulations by Wan et al.[16] have shown that $MgCl_2$ in bulk THF solvent remains coordinated by 2 THF molecules ($MgCl_2$-2THF), which we adopt as the liquid reference to compute the adsorption energies. In general, the ΔE's are always found to be very positive for all of the models considered in this study, i.e., bare $MgCl_2$ (174.8 kJ mol^{-1}), $MgCl_2$−2THF (25.0 kJ mol^{-1}), and $MgCl_2$−3THF (28.9 kJ mol^{-1}), indicating that $MgCl_2$ adsorption is not competitive with the $(MgCl)^+$ salts at equilibrium (see Figure S2 in Supporting Information).

4. DISCUSSION

To gain practical insights into the design of electrolytes capable of supporting reversible Mg deposition in Mg-ion batteries, we performed a comprehensive first-principles calculations-based adsorption study of the relevant salt and solvent species at the interface of a Mg metal surface in contact with a solution of Mg^{2+} and Cl^- dissolved in THF solvent using static adsorption calculations and *ab initio* molecular dynamics simulations. Although our model relies on a few but important assumptions, namely, a Mg metal anode free of defects and impurities, our results reveal important features of the system consistent with reversible Mg deposition and other experimental observations.

From static adsorption calculations of the anode/solvent system, THF exhibits weak interaction with Mg metal, which should leave the surface unpassivated and therefore accessible to salt adsorption. Furthermore, the adsorption calculations of $(MgCl)^+$ complexes coordinated by several THF molecules indicate that solvated salt complexes rather than solvent species are strongly preferred at the surface, which is confirmed unambiguously in the AIMD simulations. Linear poly-THF molecules, however, reported to be the product of $AlCl_3$ catalyzed THF polymerization,[10] might show larger interaction with the anode surface in comparison to THF and linear ethers.

In this investigation, we have clarified that oxygen impurities (in form of MgO) do not affect the adsorption properties of the solvent, but, as demonstrated by previous studies,[10,36] traces of other impurities such as Cl and Al can potentially react with salt species and the anode, participating in the passivation of the electrode.

Considering the Mg deposition process, once a $(MgCl)^+$ complex solvated by some (4 or 5) THF is adsorbed at the Mg surface, breaking the THF solvation shell to facilitate electron transfer is shown to be initially facile, requiring only ∼61−46 kJ mol^{-1} to remove 3 THF ligands from 5-HLW, for example. Simultaneously, the adsorbed complex adopts a conformation that brings the adsorbed Mg^{2+} ion nearer to the Mg surface, rotating from HLW to SIDE orientation, which should benefit electron transfer and eventual Mg incorporation (by maximizing the orbitals overlap between Mg^{2+} ions and Mg^0 atoms of the electrode). The energy to remove additional solvent molecules abruptly increases once there are only two remaining THF molecules, and $(MgCl)^+$ complexes solvated by 1 and 0 THF molecules do not even bind to the Mg surface, which strongly suggests that $(MgCl)^+$ coordinated by 2 THF molecules is the relevant complex involved in charge transfer, an important finding requiring further experimental verification.

The electrochemical activity of Cl as an additive to facilitate the electron transfer during multivalent metal deposition is well-known for Cu deposition, demonstrated from both a theoretical and experimental standpoint by Nagy et al.[39] The presence of Cl^- accelerates the first electron transfer from Cu^{2+} to Cu^+ in the multistep reduction of copper, and the overlap of Cl^- and Cu^{2+} orbitals eases the electron transfer mechanism by isolating the plating Cu^{2+} ions from competitive solvent interaction. In that model, it is crucial that the $Cl-Cu^{2+}$ complex preadsorb at the surface, and indications of the same behavior in this system (preferential adsorption of $(MgCl)^+$ complexes) are overall in agreement with experimental observations of reversible Mg deposition.

Although we did not explicitly consider the effect of an applied electrochemical potential to the system, the adsorption calculations in this work also shed some light on deposition events that occur post charge transfer. It is well-established that atomic and ionic Cl readily adsorb in the hollow sites of Mg metal surfaces with highly exothermic adsorption energies (−241.8 kJ mol^{-1} vs gas calculated in this work and in agreement with previous work[40]), and the observed stability of isolated Cl species in our calculations suggests that lingering Cl adsorption on a Mg surface after charge transfer may affect deposition kinetics. Indeed, recent SEM, energy-dispersive X-ray spectroscopy, and XPS measurements reveal traces of Cl (in addition to Al) at the Mg surface.[10,36] In order to keep depositing pure Mg metal at the anode, residual Cl must be continually removed, which can contribute to the plating overpotential, and we speculate that the addition of $AlCl_3$ species to the electrolyte solution may improve deposition kinetics by scrubbing the Mg anode free of Cl.[8,10] Specifically, added $AlCl_3$ can act as a shuttle for Cl^- from the anode to the cathode during Mg plating by shifting the $AlCl_3 + Cl^- \rightarrow AlCl_4^-$ reaction equilibrium; as $AlCl_3$ reacts with accumulated Cl^- at the anode surface, the AlC_4^- product is driven toward the cathode. Continual removal of chloride at the anode interface is a source of overpotential upon deposition, but in the stripping process, the additional availability of Cl^- should promote the process. During the dissolution process, the applied potential drives the charged $(MgCl)^+$ complexes to the cathode, which consequently increases the local concentration of the neutral $MgCl_2$ complexes at the anode, and, as we observe, these spontaneously dissociate into $(MgCl)^+$ and Cl^-, thus creating more carriers to drive the reaction. Overall, this creates a source of asymmetry between the deposition and stripping processes.

5. CONCLUSIONS

In conclusion, we have set to resolve the atomistic mechanisms that allow for reversible Mg electrodeposition in nonaqueous electrolytes by performing a comprehensive first-principles adsorption study at the interface of a Mg metal anode in

DOI: 10.1021/acs.chemmater.5b00389
Chem. Mater. 2015, 27, 3317−3325

contact with an electrolyte solution consisting of Mg^{2+} and Cl^- dissolved in THF (tetrahydrofuran) solvent. From an analysis of both solvent and salt adsorption from static first-principles and *ab initio* molecular dynamics calculations, we have gained a number of insights as to why this narrow class of electrolytes (magnesium−chloro salts dissolved in ethereal solvents) can function in practice: first, neither cyclic ether solvent molecules nor neutral salt complexes ($MgCl_2$-based complexes) exhibit surface-passivating behavior (although some polymeric THF shows more favorable surface interaction in comparison to cyclic THF); second, the strongest adsorbing species at the Mg interface are charged $(MgCl)^+$ complexes, which are also the active species involved in charge transfer; third, the energy to (de)solvate $(MgCl)^+$ is minimal; finally, the stable orientations of desolvated $(MgCl)^+$ complexes are also favorable for charge transfer. In future work, we plan to directly investigate the effect of an applied potential on the interfacial properties considered in this study with the goal of directly characterizing the electron-transfer mechanism upon Mg deposition and stripping.

■ ASSOCIATED CONTENT

Supporting Information

Adsorption energies for $(MgCl)^+$ and $MgCl_2$ on the Mg (0001) surface and Mg−Cl radials distribution functions for $(MgCl)^+$ salts. This material is available free of charge via the Internet at http://pubs.acs.org.

■ AUTHOR INFORMATION

Corresponding Authors

*(P.C.) E-mail: pcanepa@mit.edu.

*(G.C.) Phone: +1 617 253 1581. Fax: +1 617 253 1581. E-mail: gceder@mit.edu.

Notes

The authors declare no competing financial interest.

■ ACKNOWLEDGMENTS

This work was fully supported as part of the Joint Center for Energy Storage Research (JCESR), an Energy Innovation Hub funded by the U.S. Department of Energy, Office of Science, and Basic Energy Sciences. This study was supported by subcontract 3F-31144. We also thank the National Energy Research Scientific Computing Center (NERSC) for providing computing resources. This research used resources of the Argonne Leadership Computing Facility, which is a DOE Office of Science User Facility supported under contract DE-AC02-06CH11357, project 1309-REBatteries Revealing the Reversible Electrodeposition Mechanism in Multivalent-Ion Batteries. P.C. is grateful to Dr. E. Torres at MIT for insight in the use of the DL_POLY code and to W. D. Richards at MIT and Dr. N. Hahn at Sandia National Lab for fruitful suggestions and discussions.

■ REFERENCES

(1) Armand, M.; Tarascon, J. M. *Nature* **2008**, *451*, 652−657.

(2) Thackeray, M. M.; Wolverton, C.; Isaacs, E. D. *Energy Environ. Sci.* **2012**, *5*, 7854−7863.

(3) Aurbach, D.; Lu, Z.; Schechter, A.; Gofer, Y.; Gizbar, H.; Turgeman, R.; Cohen, Y.; Moshkovich, M.; Levi, E. *Nature* **2002**, *407*, 724−727.

(4) Van Noorden, R. *Nature* **2014**, *5*, 26−28.

(5) Cohen, Y. S.; Cohen, Y.; Aurbach, D. *J. Phys. Chem. B* **2000**, *104*, 12282−12291.

(6) Gregory, T. D.; Hoffman, R. J.; Winterton, R. C. *J. Electrochem. Soc.* **1990**, *137*, 775−780.

(7) Pour, N.; Gofer, Y.; Major, D. T.; Aurbach, D. *J. Am. Chem. Soc.* **2011**, *133*, 6270−6278.

(8) Doe, R. E.; Han, R.; Hwang, J.; Gmitter, A. J.; Shterenberg, I.; Yoo, H. D.; Pour, N.; Aurbach, D. *Chem. Commun.* **2014**, *50*, 243−245.

(9) Barile, C. J.; Spatney, R.; Zavadil, K. R.; Gewirth, A. A. *J. Phys. Chem. C* **2014**, *118*, 10694−10699.

(10) Barile, C. J.; Barile, E. C.; Zavadil, K. R.; Nuzzo, R. G.; Gewirth, A. A. *J. Phys. Chem. C* **2014**, *118*, 27623−27630.

(11) Yoo, H. D.; Shterenberg, I.; Gofer, Y.; Gershinsky, G.; Pour, N.; Aurbach, D. *Energy Environ. Sci.* **2013**, *6*, 2265−2279.

(12) Kim, H. S.; Arthur, T. S.; Allred, G. D.; Zajicek, J.; Newman, J. G.; Rodnyansky, A. E.; Oliver, A. G.; Boggess, W. C.; Muldoon, J. *Nat. Commun.* **2011**, *2*, 427.

(13) Shao, Y.; Liu, T.; Li, G.; Gu, M.; Nie, Z.; Engelhard, M.; Xiao, J.; Lv, D.; Wang, C.; Zhang, J.-G.; Liu, J. *Sci. Rep.* **2013**, *3*, 3130.

(14) Doe, R. E.; Han, R.; Gofer, Y.; Aurbach, D.; Pour, N.; Sterenberg, E. Patent WO2013096827 A1, 2013.

(15) Gizbar, H.; Vestfrid, Y.; Chusid, O.; Gofer, Y.; Gottieb, H. E.; Marks, V.; Aurbach, D. *Organometallics* **2004**, *23*, 3826−3831.

(16) Wan, L. F.; Prendergast, D. *J. Am. Chem. Soc.* **2014**, *136*, 14456−14464.

(17) Benzmayza, A.; Ramanathan, M.; Arthur, T. S.; Matsui, M.; Mizuno, F.; Guo, J.; Glans, P.-A.; Prakash, J. *J. Phys. Chem. C* **2013**, *117*, 26881−26888.

(18) Muldoon, J.; Bucur, C. B.; Gregory, T. D. *Chem. Rev.* **2014**, *114*, 11683−11720.

(19) Langreth, D. C.; et al. *J. Phys.: Condens. Matter* **2009**, *21*, 084203.

(20) Thonhauser, T.; Cooper, V. R.; Li, S.; Puzder, A.; Hyldgaard, P.; Langreth, D. C. *Phys. Rev. B* **2007**, *76*, 125112−125123.

(21) Kresse, G.; Hafner, J. *Phys. Rev. B* **1993**, *47*, 558−561.

(22) Kresse, G.; Furthmüller, J. *Phys. Rev. B* **1996**, *54*, 11169−11186.

(23) Kresse, G.; Joubert, D. *Phys. Rev. B* **1999**, *59*, 1758−1775.

(24) Nosé, S. *J. Chem. Phys.* **1984**, *81*, 511−519.

(25) Hoover, W. G. *Phys. Rev. A* **1985**, *31*, 1695−1697.

(26) MacKerell, A. D.; et al. *J. Phys. Chem. B* **1998**, *102*, 3586−3616.

(27) Todorov, I. T.; Smith, W.; Trachenko, K.; D.M, T. *J. Mater. Chem.* **2006**, *16*, 1911−1918.

(28) Mizrahi, O.; Amir, N.; Pollak, E.; Chusid, O.; Marks, V.; Gottlieb, H.; Larush, L.; Zinigrad, E.; Aurbach, D. *J. Electrochem. Soc.* **2008**, *155*, A103−A109.

(29) Matsui, M. *J. Power Sources* **2011**, *196*, 7048−7055.

(30) Ling, C.; Banerjee, D.; Matsui, M. *Electrochim. Acta* **2012**, *76*, 270−274.

(31) Aurbach, D.; Pour, N. *Corrosion of Magnesium Alloys*; Song, G.-L., Ed.; Woodhead Publishing Limited: Philadelphia, PA, 2011; Vol. *1*, Chapter 13, pp 484−515.

(32) Dreyfuss, P.; Dreyfuss, M. P. *Adv. Polym. Sci.* **1967**, *4*, 528−590.

(33) Chisholm, M. H.; Eilerts, N. W. *Chem. Commun.* **1996**, 853−854.

(34) Okoshi, M.; Yamada, Y.; Yamada, A.; Nakai, H. *J. Electrochem. Soc.* **2013**, *11*, A2160−A2165.

(35) Rajput, N. N.; Qu, X.; Sa, N.; Burrell, A. K.; Persson, K. A. *J. Am. Chem. Soc.* **2015**, *137*, 3411−3420.

(36) Gofer, Y.; Turgeman, R.; Cohen, H.; Aurbach, D. *Langmuir* **2003**, *19*, 2344−2348.

(37) Song, G.-L. *Corrosion of Magnesium Alloys: Corrosion Electrochemistry of Magnesium (Mg) and Its Alloys*; Woodhead Publishing Limited: Philadelphia, PA, 2011; Vol. *1*, pp 3−65.

(38) Namba, H.; Darville, J.; Gilles, J. M. *Surf. Sci.* **1981**, *108*, 446−482.

(39) Nagy, Z.; Blaudeau, J. P.; Hung, N. C.; Curtiss, L. A.; Zurawski, D. J. *J. Electrochem. Soc.* **1995**, *142*, L87−L89.

(40) Cheng, S.-T.; Todorova, M.; Freysoldt, C.; Neugebauer, J. *Phys. Rev. Lett.* **2014**, *113*, 136102−136107.

DOI: 10.1021/acs.chemmater.5b00389
Chem. Mater. 2015, 27, 3317−3325